

AperTO - Archivio Istituzionale Open Access dell'Università di Torino

## How do the graphenic domains terminate in activated carbons and carbon-supported metal catalysts?

**This is a pre print version of the following article:**

*Original Citation:*

*Availability:*

This version is available <http://hdl.handle.net/2318/1768849> since 2021-01-25T11:01:26Z

*Published version:*

DOI:10.1016/j.carbon.2020.07.033

*Terms of use:*

Open Access

Anyone can freely access the full text of works made available as "Open Access". Works made available under a Creative Commons license can be used according to the terms and conditions of said license. Use of all other works requires consent of the right holder (author or publisher) if not exempted from copyright protection by the applicable law.

(Article begins on next page)



# UNIVERSITÀ DEGLI STUDI DI TORINO

1  
2  
3  
4  
5  
6  
7  
8  
9  
10  
11  
12  
13

***This is an author version of the contribution published on:***

*Questa è la versione dell'autore dell'opera:*

*Carbon 169, 2020, 357-369 DOI: 10.1016/j.carbon.2020.07.033*

***The definitive version is available at:***

*La versione definitiva è disponibile alla URL:*

<https://www.sciencedirect.com/science/article/pii/S000862232030693X>

# 1 **How do the graphenic domains terminate in activated carbons** 2 **and carbon-supported metal catalysts?**

3 Eleonora Vottero,<sup>1,2</sup> Michele Carosso,<sup>1</sup> Mónica Jiménez-Ruiz,<sup>2</sup> Riccardo Pellegrini,<sup>3</sup> Elena Groppo,<sup>1</sup>  
4 Andrea Piovano<sup>2,\*</sup>

5 1) Department of Chemistry, NIS Centre and INSTM, University of Turin, Via G. Quarello 15/A,  
6 Turin, I-10135, Italy;

7 2) Institut Laue-Langevin (ILL), 71 Avenue des Martyrs, 38042 Grenoble, France;

8 3) Chimet SpA–Catalyst Division, Via di Pesciola 74, Viciomaggio Arezzo, I-52041, Italy  
9

## 10 **Abstract**

11 This work is focused on the determination of the most likely border morphologies in the H-terminated  
12 graphenic domains that constitute activated carbons, focusing on four different carbons and six  
13 supported-metal catalysts. Among the available characterization techniques, Inelastic Neutron  
14 Scattering spectroscopy provides detailed vibrational spectra containing the fingerprint of the  
15 terminal C-H groups of carbon materials. From the experimental spectra, we observed clear  
16 differences among carbons having different origin, and a systematic decrease in the integrated area  
17 upon metal deposition that linearly scales with the nanoparticles dispersion. Density Functional  
18 Theory simulations are fundamental to assign the experimental bands to specific species. Thus, an  
19 extended simulation work on both regular and defective aromatic models was carried out, providing  
20 the inelastic neutron scattering fingerprint of a large number of different C-H terminations. By fitting  
21 the experimental spectra with a linear combination of the simulated spectra, it was possible to quantify  
22 the concentration of each terminal C-H geometry in the samples, and to identify the species most  
23 affected by the metal nanoparticles deposition. Specific benzene rings exposing a single C-H group  
24 appear to have a decisive role in the interaction with the metal nanoparticles and their deposition  
25 procedure.

## 1 **1. Introduction**

2 Activated carbons are large surface area carbonaceous materials obtained from the pyrolysis and  
3 subsequent activation of several natural bio-polymeric precursors (such as wood, peat or coconut  
4 shells) [1]. They are widely employed as adsorbent or storage materials [2, 3], as supports in  
5 heterogeneous catalysis [4] or as catalysts on their own [5-9], and also for innovative applications  
6 such as lithium batteries [10]. From a micro-structural point of view, activated carbons are constituted  
7 by small and heterogeneously sized and shaped graphenic domains mainly terminated by C-H groups,  
8 which also exhibit variable amounts of functional groups containing heteroatoms (such as oxygen or  
9 nitrogen) and a certain degree of defectivity. All these properties, as well as the surface area and  
10 porosity, are largely affected by the nature of the starting precursor and by the activation procedure  
11 [11, 12]. Altogether, the textural, morphological and surface properties of an activated carbon have  
12 dramatic effects on their catalytic performances. As an example, we recently demonstrated that, for  
13 Pd-based catalysts supported on activated carbons, oxygen-containing functional groups at the carbon  
14 surface favour the hydrogenation of polar substrates, while they are detrimental to the hydrogenation  
15 of nonpolar substrates [13].

16 It emerges that a detailed understanding of the microscopic structure of activated carbons is  
17 essential to optimize their performance for a specific application, in particular for catalysis. Among  
18 the numerous techniques that can be employed for their characterization [14], Inelastic Neutron  
19 Scattering (INS) spectroscopy stands up as one of the most powerful methods to determine the nature  
20 of the C-H terminations of the graphenic domains. INS is a vibrational spectroscopy that exploits  
21 neutrons to excite molecular and/or atomic vibrations inside materials, and the intensity of the signal  
22 is proportional to the neutron scattering cross section of the atoms involved in the vibrational mode  
23 and to their displacement with respect to their equilibrium position. Since hydrogen displays both the  
24 largest neutron scattering cross section and large displacements due to its lightweight, this technique  
25 is particularly sensitive to the hydrogen-containing species in a material. This is the reason why INS  
26 spectroscopy has been successfully employed in the study of several carbon-based materials including  
27 activated carbons [15-18], carbon blacks [16, 19], coals [16, 20], glassy carbon [16, 21] or reduced  
28 graphene oxides [22, 23]. Despite the huge variety of properties displayed by these materials, their  
29 structure down to the atomic scale is to some extent similar, and so are their main spectral features.

30 Nevertheless, the bands assignment in an INS spectrum can be tricky. The reason is that this  
31 technique has formally no selection rules allowing, at least in principle, the detection of all the  
32 vibrational modes. Therefore, INS spectra of complex and heterogeneous samples containing high  
33 amounts of hydrogenous species usually show a large number of bands, whose assignment becomes  
34 challenging. The employment of computational methods to simulate the INS spectra can be extremely

1 helpful and, among the available computational chemistry approaches, DFT simulations  
2 demonstrated to provide reliable results at reasonable computational costs. Albers et al. were the first  
3 authors who adopted a combined INS and computational approach to study activated carbons [15].  
4 Their analysis showed that the fingerprint region of the C-H out-of-plane bending modes (800-1000  
5  $\text{cm}^{-1}$ ) is the one mostly affected by differences in the microstructure of activated carbons. More  
6 recently, some of the authors revisited the interpretation of INS spectral features in the fingerprint  
7 region of activated carbons [24]. In particular, a more precise assignment of the contributions from  
8 different C-H terminations of the graphenic domains (including zigzag and armchair edges, as well  
9 as corners) was proposed. Still, so far the interpretation of the C-H vibrational features in activated  
10 carbons was limited to the comparison of experimental data of mediocre quality with simple  
11 theoretical models consisting of a few aromatic rings completely terminated by C-H groups, which  
12 are not representative of the real complexity of activated carbons.

13         Thanks to recent advances in INS instrumentations, the spectra collected on modern neutron  
14 spectrometers on well-prepared samples show an unprecedented signal-to-noise ratio, allowing for a  
15 more precise interpretation of the spectral features and for a higher reliability for the spectral  
16 differences. As an example, Cavallari et al. were recently able to collect high quality INS spectra of  
17 regular and defective hydrogenated graphene samples [23]. Combining the experimental spectra and  
18 DFT simulations, they identified the INS fingerprints of C-H groups at the periphery of the graphenic  
19 planes as well as inside holes. They quantified the two species abundance and they were able to  
20 monitor the migration of H atoms to adjacent vacant sites as a function of the temperature. Similarly,  
21 in our recent work we investigated a 5 wt.% Pt catalyst supported on an activated carbon in the  
22 presence of different amounts of  $\text{H}_2$  [18]. The collected INS data allowed for a detailed difference  
23 analysis between the spectrum of the catalyst and that of the carbon support, as well as between the  
24 spectrum of the catalyst in the absence and in the presence of  $\text{H}_2$ . With this approach, we were able  
25 to assess more specifically the location of the Pt nanoparticles on the carbon support and to highlight  
26 the occurrence of hydrogen spillover from the Pt nanoparticles to the support. Despite the low Pt  
27 loading, we were also able to detect surface Pt-hydride species forming and modifying upon  
28 increasing the  $\text{H}_2$  concentration. These examples demonstrate that nowadays we can rely on the fact  
29 that differences in the INS spectra of carbon-based samples under different conditions can be  
30 interpreted as clear structural modifications. At the same time, differences between measured and  
31 computed INS spectra can be considered as the result of a lack of specific features in the theoretical  
32 model.

33         In this work, we propose a systematic DFT simulation study of a large number of graphenic  
34 model systems, aimed at providing the INS fingerprints of a wide range of different C-H termination

1 geometries, as well as at understanding how they are affected by the presence of defects. The  
2 theoretical results are used for interpreting the experimental INS spectra of four physically activated  
3 carbons, deriving from wood and peat, and of a series of carbon-supported Pd- and Pt-based catalysts  
4 employed for hydrogenation reactions of industrial relevance. In principle, the same methodology  
5 can be easily extended to other classes of carbon-based materials. In this respect, we wish that this  
6 paper might become a guide for researchers who want to adopt similar approaches in material science.

## 7 **2. Experimental**

### 8 **2.1. Activated carbon samples**

9 The four activated carbons investigated in this work were commercially available carbons and were  
10 provided by the Catalyst Division of Chimet S.p.A. All of them were physically activated with steam,  
11 but they derive from different raw materials, wood (hereafter labelled as CwA and CwB) and peat  
12 (labelled as CpA and CpB). The ash content of the four carbons was determined by calcination and  
13 is below 2 wt% in the two carbons of wood origin, and of about 3 wt% for CpA and 5.5 wt% for CpB.  
14 Table 1 summarizes the specific surface area ( $SSA_{BET}$ ) and micropore volume ( $V_{micro}$ ) of the four  
15 carbons, as determined by  $N_2$  physisorption measurements. The adsorption isotherms for the four  
16 supports are reported in the supporting information, Figure S1. **The catalysts supports are activated  
17 carbons derived from natural sources and, as such, they are characterized a certain degree of  
18 heterogeneity in terms of carbon structure, morphology and porosity intrinsic in the natural source.  
19 Representative SEM images of the four activated catalysts at two different magnifications are  
20 reported in Figure S2 in Supporting Information to show the structural inhomogeneity of the carbons  
21 at the  $\mu m$  scale.**

22 Table 1. Properties of the activated carbons investigated in this work: raw material, activation method, specific surface  
23 area (SSA) as determined by  $N_2$  physisorption measurements by applying the BET method and the corresponding volume  
24 of the micropores ( $V_{micro}$ ).

<b>Sample</b>	<b>Origin</b>	<b>Activation</b>	<b><math>SSA_{BET}</math> (<math>m^2g^{-1}</math>)</b>	<b><math>V_{micro}</math> (<math>cm^3g^{-1}</math>)</b>
<b>CwA</b>	wood	steam	1018	0.63
<b>CwB</b>	wood	steam	1325	0.65
<b>CpA</b>	peat	steam	903	0.49
<b>CpB</b>	peat	steam	882	0.52

### 25 **2.2. Catalysts preparation**

26 All the catalysts were prepared in the Chimet S.p.A. laboratories. Two Pd-based catalysts (5 wt% Pd  
27 loading) were prepared using CwA as a support, following the deposition–precipitation method as  
28 reported elsewhere [25, 26].  $Na_2PdCl_4$  was used as the metal precursor and  $Na_2CO_3$  as the basic agent.  
29 The two Pd/CwA catalysts differ in the reduction step: in one case, after the deposition of palladium

1 as hydroxide, a pre-reduction was carried out by means of HCOONa at 55 °C for 1 h, followed by  
 2 water washing in order to remove residual chlorine and drying at 120 °C overnight. In the other case,  
 3 no pre-reduction was performed and the Pd deposition step was directly followed by washing and  
 4 drying. The two catalysts are labelled as Pd(R)/CwA and Pd(NR)/CwA, where (R) and (NR) stand  
 5 for reduced and not-reduced, respectively.

6 A series of Pt-based catalysts (5 wt% Pt loading) were prepared using the four activated  
 7 carbons as supports, following a deposition-precipitation method similar to the one reported by  
 8 Kaprielova et al. [27]. A pre-reduction was carried out also in this case by means of HCOONa at 80  
 9 °C for 1 h, followed by water washing and drying at 120 °C overnight. These catalysts are labelled  
 10 with Pt(R), followed by the name of the carbon employed as support. The main characteristics of all  
 11 the considered catalysts are summarized in Table 2. In all the cases, the metal dispersion was  
 12 evaluated by means of CO chemisorption. The measurements were performed at 50 °C using a  
 13 dynamic pulse method on samples pre-reduced in H<sub>2</sub> at 120 °C [28]. In a typical experiment, the  
 14 catalyst (200 mg) is loaded inside the U-tube, heated in He up to 120 °C (heating rate of 10 °C min<sup>-1</sup>),  
 15 reduced in H<sub>2</sub> for 30 min, and finally cooled to 50 °C in He (cooling rate of 10 °C min<sup>-1</sup>). A CO/metal  
 16 average stoichiometry of 1 was assumed to calculate the metal dispersion for both the metals, as  
 17 widely documented [29]. **The discussed heterogeneity of the support does not point to a poor quality  
 18 of the commercial catalysts. To verify that the supported metal nanoparticles are in homogeneous in  
 19 terms of morphology (spherical-like particles) and display a narrow particle size distribution, we  
 20 recorded TEM micrographs on Pd/CwA and Pt/CwA catalysts (see figure S3 in Supporting  
 21 information for representative images).**

22 Table 2. Properties of the catalysts studied in the current work: the activated carbon support type, the deposited metal, the  
 23 eventual presence of a pre-reduction step and the metal nanoparticles dispersion (evaluated by means CO chemisorption).

<b>SAMPLE</b>	<b>SUPPORT</b>	<b>METAL</b>	<b>PRE-REDUCED</b>	<b>DISPERSION (%)</b>
<b>PD(NR)/CWA</b>	CwA	Pd	No	24
<b>PD(R)/CWA</b>	CwA	Pd	Yes	24
<b>PT(R)/CWA</b>	CwA	Pt	Yes	72
<b>PT(R)/CwB</b>	CwB	Pt	Yes	77
<b>Pt(R)/CpA</b>	CpA	Pt	Yes	71
<b>Pt(R)/CpB</b>	CpB	Pt	Yes	69

### 24 2.3. INS measurements

25 The INS measurements were performed on the LAGRANGE spectrometer at ILL in Grenoble  
 26 (France) [30-32]. The INS spectra were collected in the 24-1020 cm<sup>-1</sup> range, with a resolution of  $\Delta E/E$   
 27 of about 2%. The spectra were recorded at 20 K to reduce the thermal effects that broaden the spectral  
 28 features. The raw data were opportunely reduced to the scattering function  $S(\omega)$  and plotted versus

1 energy transfer (in units of  $\text{cm}^{-1}$ ). In order to ensure an easy comparison of each catalyst with its  
2 respective support, we renormalized the intensity of the former to match the same background  
3 intensity of the latter at  $1020 \text{ cm}^{-1}$ . The analysis, described in section 3.1, confirmed that contributions  
4 other than the background are negligible in this region.

5 Prior to the measure, all the samples were outgassed at  $120 \text{ }^\circ\text{C}$  in dynamic vacuum  
6 (equilibrium pressure below  $10^{-4}$  mbar) in order to remove the physisorbed water, and any further  
7 manipulation was performed within an Ar-filled glovebox in order to avoid any contamination with  
8 air moisture. A weighted amount of each sample (in the order of about 2-3 g) was inserted in a  
9 cylindrical Al-cell (4 cm high, 16 mm diameter) sealed with In-wire and then measured.

### 10 **3. Theoretical methods**

#### 11 **3.1. DFT simulations of the INS spectra**

12 The DFT simulations of the INS spectra were performed employing the CRYSTAL17 software [33]  
13 in combination with the aClimax software [34]. A good compromise between results reliability and  
14 computational cost was found in the combination between the B3LYP hybrid functional [35, 36] and  
15 the 6-31G\*\* basis set, as also proposed in the literature for similar systems [37, 38]. Some models  
16 presented an open shell electronic configuration, for which the UB3LYP method was chosen. The  
17 general models employed for simulating the structure of activated carbons consist in polycyclic  
18 aromatic systems displaying different geometries and extensions, with hydrogen atoms used to  
19 saturate dangling bonds at edges and corners. Similar models have been already adopted in the  
20 literature to simulate the vibrational properties of the graphenic domains in carbon-based materials  
21 [15, 24, 38]. A total of 16 regular and 6 defective H-terminated different structures are reported in  
22 this work (see Figure 3 and Figure 8), while a greater number of them have been effectively simulated.  
23 The geometry of all the models was fully optimized, and successively a calculation of the vibrational  
24 modes was performed. All the structures were categorized as true energy minima by the absence of  
25 imaginary frequencies. The condition for the SCF convergence was set to  $10^{-8}$  and  $10^{-10}$  hartrees  
26 during geometry optimization and frequency calculations, respectively. In order to ensure the best  
27 accuracy, very thig values (8 8 8 25 50) have been set for the five CRYSTAL17 integrals screening  
28 tolerance.

29 The output of the frequency calculation was used to simulate the INS spectra by employing  
30 the aClimax software [34]. Simulations of higher order transitions and phonon wings contributions  
31 were also performed, but not included into the final simulated spectra because they generated features  
32 that were not experimentally observed. The contribution of specific border fragments to the overall  
33 INS spectrum was simulated by manually setting the scattering cross section of all the atoms not

1 included within the interested fragment to 0 barns. For a better comparison with the experimental  
2 spectra, the calculated frequencies have been scaled: the employed scaling function was obtained  
3 through a least squares linear regression of the experimental and calculated frequencies for the  
4 benzene molecule, as proposed in reference [39], resulting in the scaling function  $\nu_{\text{scaled}}=22.1 +$   
5  $0.9543\nu_{\text{calculated}}$ .

### 6 **3.2. Linear combination analysis**

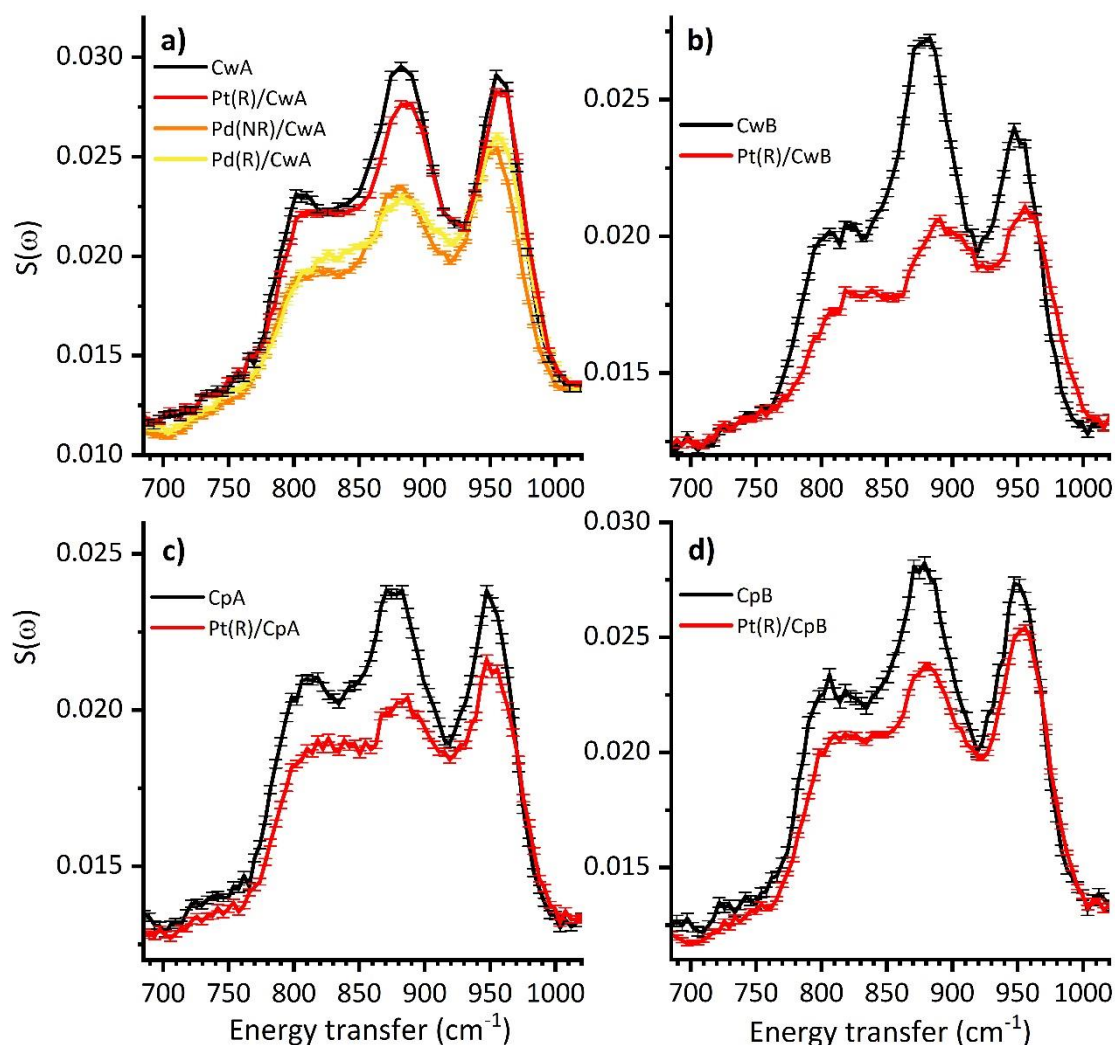
7 To evaluate the weight of each simulated C-H terminal geometry in the experimental spectra, a linear  
8 combination fit analysis was performed. Each theoretical C-H contribution was normalised to the  
9 intensity of a single C-H group, averaged over similar models and then multiplied for a weight  
10 coefficient, whose final value in the best-fit solution is proportional to the concentration of that  
11 species in the sample. To compare among the values obtained for different samples, the optimised  
12 values of the sum of these coefficients were normalised to 1 for each support, while the catalysts were  
13 normalised respect to the corresponding support. A small multiplicative scaling factor  $s$  ( $0.99 < s <$   
14  $1.01$ ) was introduced on the frequency to adjust for small shifts along the horizontal axis.

15

## 16 **4. Results and discussion**

### 17 **4.1. Experimental INS spectra**

18 In the analysis of the experimental INS spectra, we decided to focus our attention on the 690 – 1020  
19  $\text{cm}^{-1}$  range, characteristic of the out-of-plane C-H bending vibrations [15-18, 24]. This is the region  
20 of the spectra that exhibits the greatest variations among the samples, and thus can be considered as  
21 the INS fingerprint of C-H terminations in the activated carbon samples. The spectra in the extended  
22 range 200-1020  $\text{cm}^{-1}$  are reported in Figure S4, S5, S6 and S7 in the supporting information, while  
23 an overall assignment of all the observed bands is described elsewhere [17]. Figure 1 shows the INS  
24 spectra of the four activated carbons and of the corresponding Pd- and Pt- based catalysts in the 690  
25 – 1020  $\text{cm}^{-1}$  range. All the spectra are characterized by three main bands centred at similar positions  
26 (ca. 800, 880 and 955  $\text{cm}^{-1}$ , with a tail extending at 750  $\text{cm}^{-1}$ ). Differences in the relative intensity of  
27 the three bands are observed between carbons derived from different raw materials (Figure 1a-d), but  
28 also between carbons having the same origin (e.g. for CwB, Figure 1b, the band at ca. 880  $\text{cm}^{-1}$  is  
29 distinctively more intense than for CwA, Figure 1a). These variations are expected to be caused by  
30 changes in the relative concentration of different C-H terminal geometries of the graphenic domains  
31 within the investigated samples.



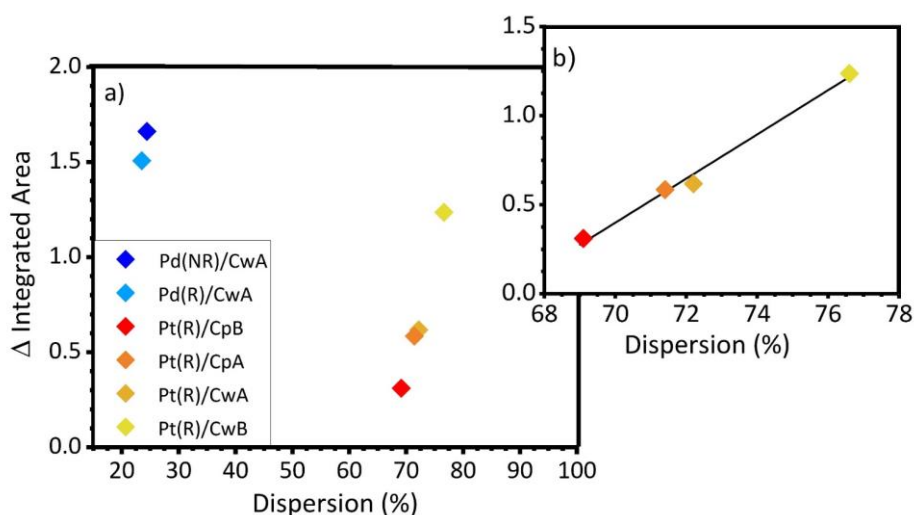
1

2 Figure 1. Experimental INS spectra of the four activated carbons (black) and of the corresponding Pd- and Pt-based  
 3 catalysts, as measured at the LAGRANGE spectrometer at ILL. The spectra are shown in the 690 – 1020  $\text{cm}^{-1}$  range,  
 4 characteristic of the out-of-plane C-H bending vibrations. The intensity of the catalysts' spectra is normalised to the one  
 5 of the support to the value of the background.

6 Variations are also observed when comparing the INS spectra of the Pd and Pt catalysts (red,  
 7 orange and yellow spectra in Figure 1a-d) with those of the parent carbons (black spectra). The  
 8 observed changes are very similar irrespective of the carbon type, of the metal and of the metal  
 9 deposition method. A decrease in intensity of all the three bands is observed, more pronounced for  
 10 the one centred at 880  $\text{cm}^{-1}$  than for the others. This behaviour could be the result of the interaction  
 11 of Pt and Pd nanoparticles with the C-H terminations of graphenic domains in the carbon support,  
 12 and it highlights that some types of C-H terminations are more affected than others. Similar variations  
 13 were recently reported for the Pt(R)/CwA catalyst compared to the bare carbon support, and  
 14 interpreted as an evidence that the Pt nanoparticles can be located at the edges of the  $\text{sp}^2$  graphenic  
 15 domains [18].

16 The absolute intensity of INS spectra is directly proportional to the hydrogen concentration  
 17 within each sample [15, 17]. In this respect, CwA is the activated carbon displaying the highest

1 hydrogen concentration, closely followed by CwB and CpA, while CpB shows a much lower amount  
 2 of hydrogen in respect to the others. Albers *et al.* [15] demonstrated that the integrated area of the  
 3 spectra in the C-H bending region linearly scales with the H concentration in the sample. We have  
 4 thus decided to use the integrated area of the spectra in the out-of-plane bending region ( $690-1020$   
 5  $\text{cm}^{-1}$ ) to evaluate the H concentration within each of the samples. The variation in the integrated area  
 6 of the spectra of all the catalysts with respect to the bare carbon support was calculated and plotted  
 7 against the metal nanoparticles dispersion, as shown in Figure 2. For the Pt catalysts, the decrease in  
 8 the integrated area (i.e. in the H concentration) is directly proportional to the dispersion of the metal  
 9 nanoparticles, as shown in Figure 2b. This observation suggests that smaller the nanoparticles, higher  
 10 is their interaction with the borders of the graphenic platelets. The two Pd catalysts instead exhibit  
 11 large variations in H content albeit their low dispersion, as shown in Figure 2a, suggesting that Pd  
 12 nanoparticles interact more with the C-H terminations than the Pt ones.



13

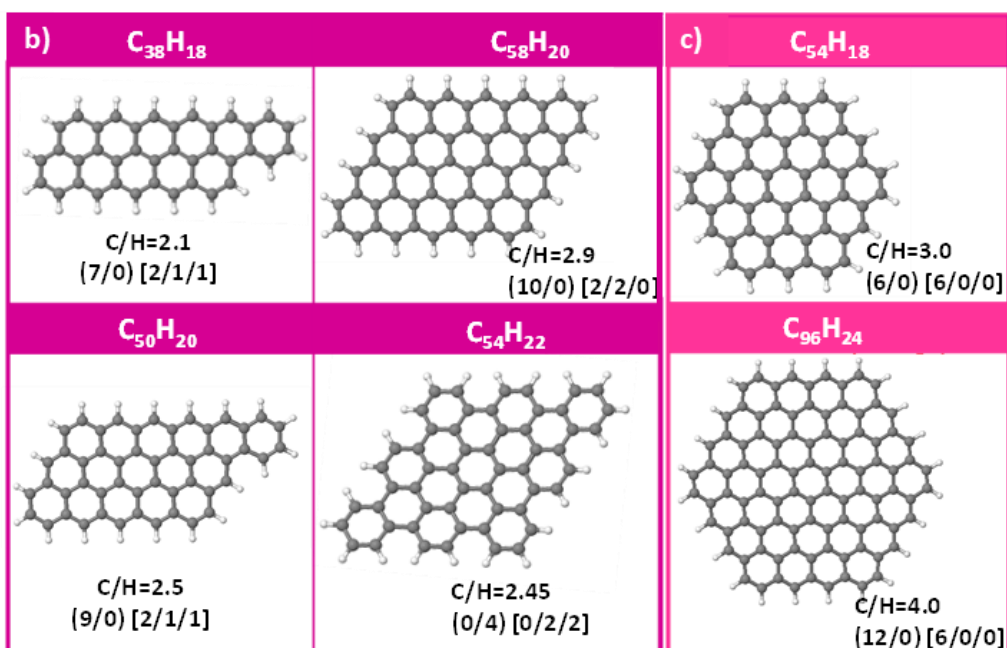
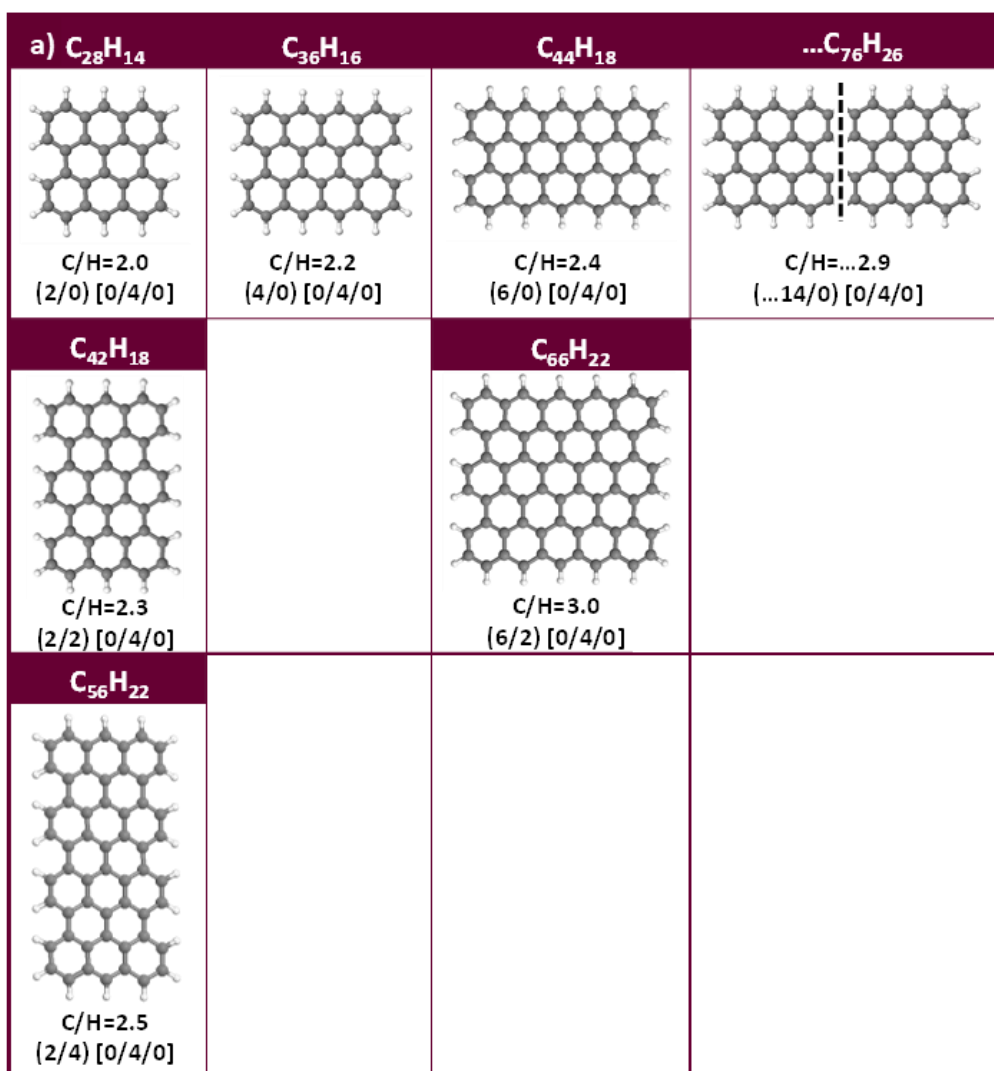
14 Figure 2: a) Difference in the integrated area of the INS spectra in the out-of-plane bending region ( $690-1020 \text{ cm}^{-1}$ )  
 15 between the bare carbon support and the corresponding catalysts versus the metal dispersion. b) Magnification of the Pt  
 16 catalysts points: a linear trend can be observed.

#### 17 4.2. DFT simulations of the INS spectra for regular C-H terminations

18 The three bands observed in the experimental spectra shown in the previous paragraph are attributed  
 19 to vibrations of specific C-H terminal geometries. The observed changes in relative intensity reflect  
 20 a change in their concentration. A qualitative bands assignment was done previously on the basis of  
 21 DFT calculations performed on very simple aromatic models [24], that cannot account for the  
 22 heterogeneity of real samples. For this reason, we underwent a large and systematic theoretical study  
 23 aimed at exploring a much wider range of possible sizes, border geometries and terminations, with  
 24 the aim to perform a quantitative analysis of the experimental spectra.

1           The models initially employed for the new DFT simulation of the INS spectra consist in  
2 regular aromatic structures where all the carbon atoms are  $sp^2$  hybridized and all the terminations are  
3 saturated by H atoms. Their geometry can be described in terms of extended regular borders and  
4 corners. Extended regular borders can show a regular sequence of benzene rings exposing a single C-  
5 H group named zigzag edge (Z), or an alternation of benzene rings exposing two adjacent C-H groups  
6 named armchair edge (A). The intersection of two regular borders generates a corner site that can  
7 present two, three or four adjacent C-H groups and will be labelled as *duo* (D), *trio* (T) or *quatro* (Q),  
8 respectively, following the nomenclature proposed by Zander for substituted benzenes [40, 41]

9           The models have been categorized in Figure 3 as a function of their shape, i.e. the relative  
10 extension of Z and A edges. Figure 3a summarizes the models having a rectangular shape, which is  
11 defined by two zigzag and two armchair edges and by four T corners. Moving in the horizontal  
12 direction, the Z edge increases in length while keeping constant the dimension of the A edge; moving  
13 in the vertical direction, the A edge increases, instead. Figure 3b displays models having a  
14 parallelogram shape, which is defined by a single type of edge, either Z ( $C_{38}H_{18}$ ,  $C_{58}H_{20}$ ,  $C_{50}H_{20}$ ), or  
15 A ( $C_{54}H_{22}$ ). For the  $C_{38}H_{18}$  and  $C_{50}H_{20}$  models, an aromatic ring was added in order to break the  
16 symmetry, resulting in the addition of a corner of Q type. In this category, the typologies of corners  
17 are more varied, resulting in an alternation of D and T corners in the models featuring Z edges and of  
18 T and Q corners for the model featuring A edges. Finally, Figure 3c shows two hexagonal models,  
19 the latter being also the largest model adopted in this work, showing only Z edges alternating with D  
20 corners. The relative abundance of Z and A edges, as well as of D, T, and Q corners is reported in  
21 Figure 3 for all the models in parenthesis, following the notation (Z/A) for the edges, and [D/T/Q] for  
22 the corners.

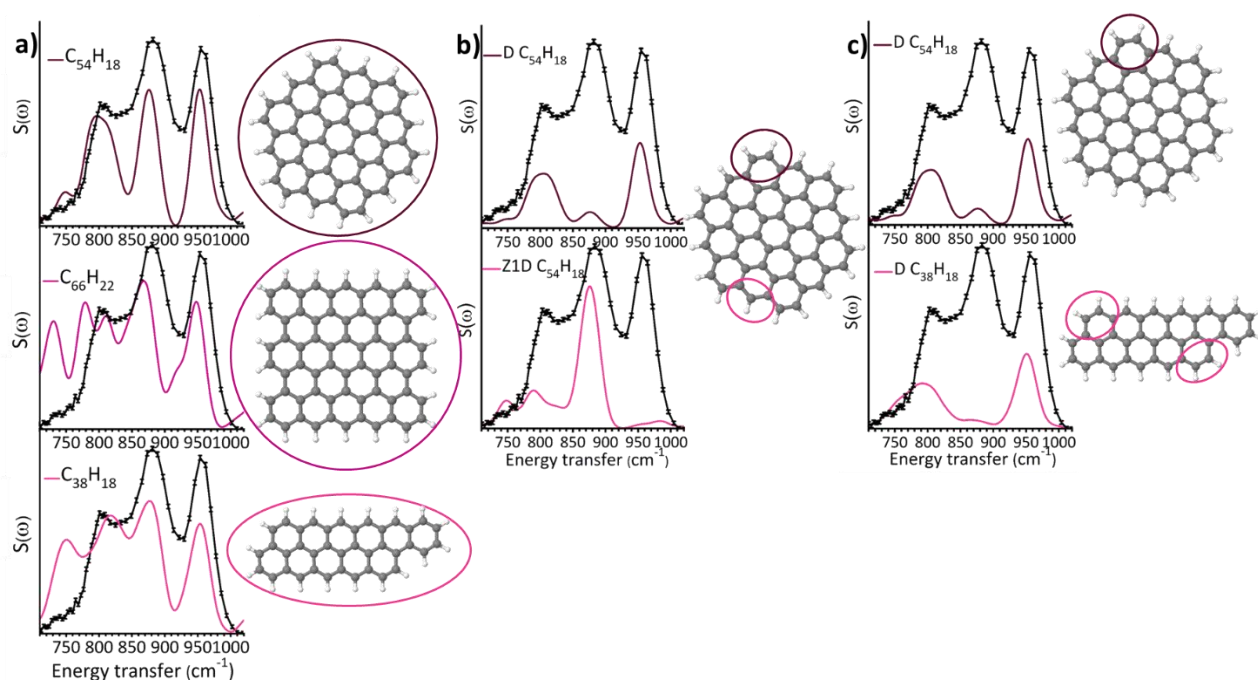


1  
2 Figure 3. Overview of the models simulated in this work, categorized in terms of their shape. For all the models, the C/H  
3 ratio is indicated, as well as the relative abundance of zigzag and armchair edges (Z/A), and of *duo*, *trio* and *quatro*  
4 corners [D/T/Q].

1 Figure 4a shows three representative simulated INS spectra for three models having different  
 2 size and shape, in comparison with the experimental spectrum of CwA, taken in the following as a  
 3 reference. As expected, all the models contribute with some bands in the 690 – 1020  $\text{cm}^{-1}$  range.  
 4 However, different models clearly show distinct bands in terms of number, position and relative  
 5 intensity. The simulated INS spectrum of  $\text{C}_{54}\text{H}_{18}$  is the closest to the experimental one in terms of  
 6 both bands positions and relative intensity, while the INS spectra of  $\text{C}_{66}\text{H}_{22}$  and  $\text{C}_{38}\text{H}_{18}$  evidently  
 7 show bands not present in the experimental one. This demonstrated that the model geometry has a  
 8 dramatic effect on the result.

9 In order to better analyse the characteristic spectral features of each C-H termination portion  
 10 in the models, their contributions to the overall simulated spectra were separated and analysed  
 11 individually. For example, model  $\text{C}_{54}\text{H}_{18}$  includes two distinct terminal C-H geometries (Z edges and  
 12 D corners), whose spectral contributions are reported in Figure 4Figure 4b. It is evident that the two  
 13 C-H terminations display significantly different spectral features: the D corners are responsible for  
 14 the appearance of the two bands at 800 and 955  $\text{cm}^{-1}$ , while the C-H at the Z edges are mainly  
 15 responsible for the band at 880  $\text{cm}^{-1}$ . However, D corners belonging to two different models are  
 16 characterized by very similar spectral features as shown in Figure 4c. Analogous considerations apply  
 17 for the other models and terminations, making it clear that the INS spectra of each C-H termination  
 18 in the 690 – 1020  $\text{cm}^{-1}$  range mostly depend on local geometry and are only marginally affected by  
 19 the general structure of the model. This does not hold for the rest of the spectral range, where the  
 20 vibrational modes often display collective features, resulting in spectra reflecting the geometry of the  
 21 whole model more than the single C-H terminations. [24]

22



23

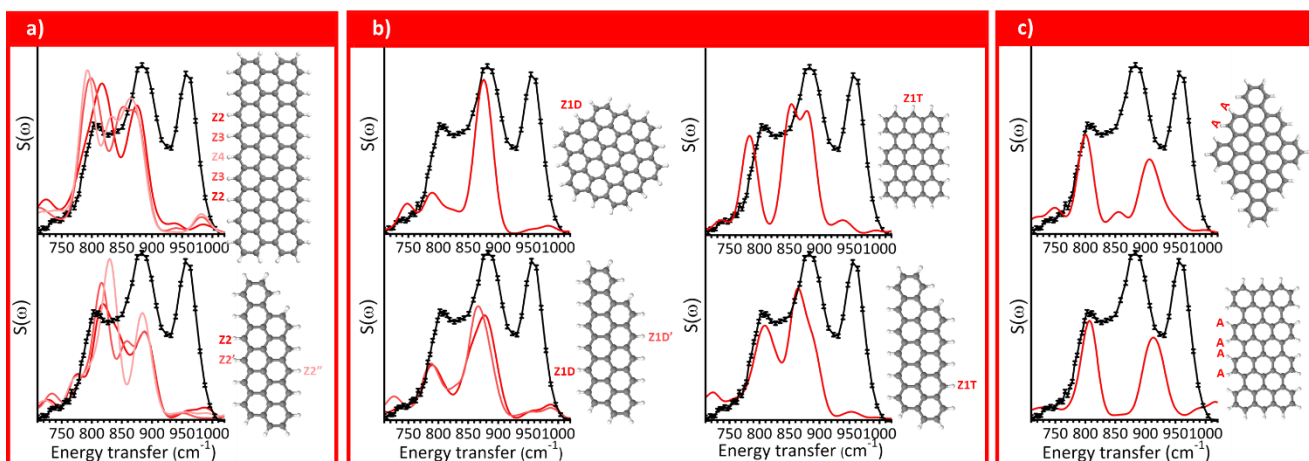
1 Figure 4. Part a): Comparison between the simulated INS spectra of three models having different shape and the  
2 experimental spectrum of CwA (black). Different model geometries result in different simulated spectra. Part b): The  
3 partial contribution of the two types of C-H termination characterizing the  $C_{54}H_{18}$  model in comparison to the  
4 experimental spectrum of CwA (black). Part c): Simulated spectral contribution of two D corners belonging to two  
5 different models, compared to the experimental spectrum of CwA (black).

6 On these bases, we systematically investigated the INS contributions of specific C-H terminal  
7 geometries in the  $690 - 1020 \text{ cm}^{-1}$  range. Five different classes of C-H terminations were identified,  
8 and their partial INS spectra were simulated and compared.

9 **Extended zigzag borders** give rise to a couple of INS signals centred at ca.  $800 \text{ cm}^{-1}$  and  $880$   
10  $\text{cm}^{-1}$ , which are attributed to the out-of-plane bending mode,  $\delta(\text{C-H})$ , in which adjacent C-H sites  
11 vibrate out-of-phase and in-phase, respectively. Being a correlated mode, the exact position of these  
12 two bands and their relative intensity depend on the extension of the border or, in other words, on the  
13 distance of the C-H groups from the corners. For the sites located at the extremities, it also depends  
14 on the geometry of adjacent sites. Figure 5a and b show some representative spectra of zig-zag borders  
15 belonging to different models, whereby each C-H group has been labelled as Z, followed by a number  
16 indicating the distance from the corner (e.g. Z2 is the second C-H belonging to the regular zigzag  
17 border starting counting from the corner). For Z1 sites (i.e. those adjacent to a corner) another letter  
18 is added to describe the adjacent corner (D = *duo*, T = *trio*). Trying to generalize, the spectra of Z  
19 sites far from the corners tend to converge, as shown in Figure 5a (e.g. the spectra of Z3 and Z4 sites  
20 in  $C_{76}H_{26}$  are very similar). In these cases, usually the band at ca.  $800 \text{ cm}^{-1}$  is more intense than that  
21 at  $880 \text{ cm}^{-1}$ . Z2 sites tend to show the same two  $\delta(\text{C-H})$  bands, shifted at higher energy transfer. The  
22 spectra of Z1 sites are more scattered depending on the model (Figure 5b), and mainly depend on the  
23 type of the adjacent corner. For the Z1D sites (i.e. Z1 sites close to a *duo* corner) the band at ca.  $800$   
24  $\text{cm}^{-1}$  is largely reduced in intensity and the spectra are dominated by the band at  $880 \text{ cm}^{-1}$ . In the  
25 spectra of Z1T sites the band at ca.  $870 \text{ cm}^{-1}$  is usually split in two components and more intense than  
26 that at ca.  $800 \text{ cm}^{-1}$ .

27 The spectra of **extended armchair borders** (Figure 5c) are generally characterized by two  
28 bands centred at ca.  $810 \text{ cm}^{-1}$  and  $920 \text{ cm}^{-1}$ , corresponding to the out-of-plane  $\delta(\text{C-H})$  modes of the  
29 two adjacent C-H sites that vibrate in-phase and out-of-phase, respectively. In this case, the final  
30 spectrum is almost the same irrespective of the length of the border and the geometry of the platelet.

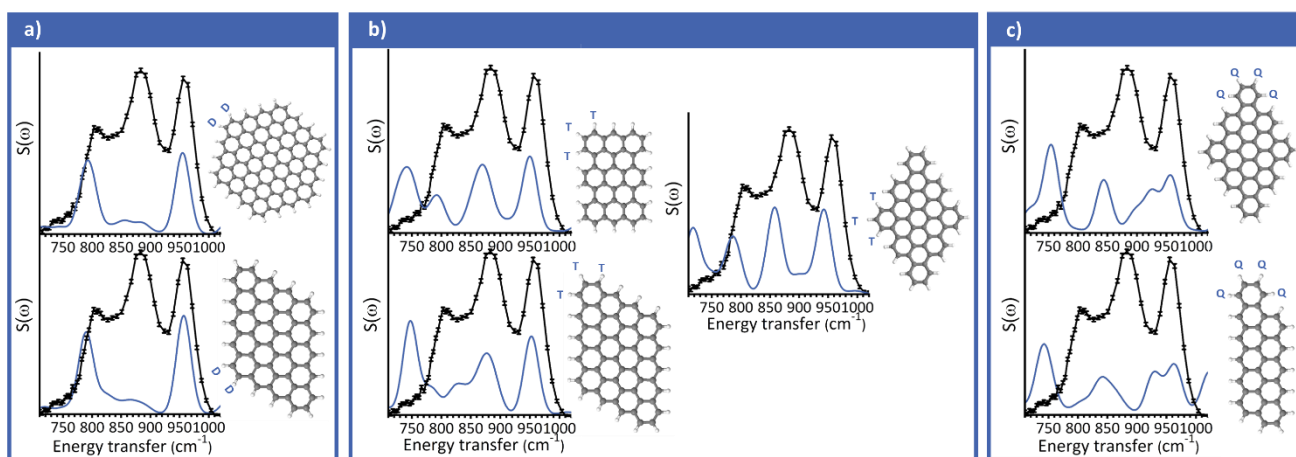
31



1  
2 Figure 5. Part a): Representative contributions of different types of C-H terminations at zig-zag borders (Z sites) far from  
3 the corners and belonging to different models. Part b): representative contributions of Z1 C-H terminations differing in  
4 the type of adjacent corner (D = duo, T = trio) and belonging to different models. Part c): Representative contributions of  
5 different C-H terminations at armchair borders (A sites).

6  
7 A **duo corner** (Figure 6a) consists in a benzene ring at a corner position exposing two adjacent C-H  
8 groups. The INS spectra of *duo* corners are all characterized by two bands centred at ca. 795 and 960  
9  $\text{cm}^{-1}$ , corresponding to the out-of-plane  $\delta(\text{C-H})$  modes of the two adjacent C-H groups that vibrate in-  
10 phase and out-of-phase, similarly to the extended armchair border case. However, the spectra of D  
11 and A sites can be easily distinguished on the bases of the position of the two bands, evidently more  
12 spaced for D corners than for A edges. A **trio corner** (Figure 6b) consists in a benzene ring exposing  
13 three adjacent C-H groups. The vibrational modes of the three C-H groups are strongly correlated,  
14 and usually four bands are observed, the first two at ca. 750 and 800  $\text{cm}^{-1}$  (in some cases the 800  $\text{cm}^{-1}$   
15  $^{-1}$  band appears as a shoulder of the former), the third at 850 and the fourth at 950  $\text{cm}^{-1}$ . The relative  
16 intensities of the bands appear to be affected by the typology of adjacent extended borders (either Z  
17 or A). Finally, a **quatro corner** (Figure 6c) consists in a benzene ring exposing four adjacent C-H  
18 sites. The spectra of Q corners display four bands centred at about 740, 840, 930 and 960  $\text{cm}^{-1}$  and  
19 are almost invariant with the model.

20

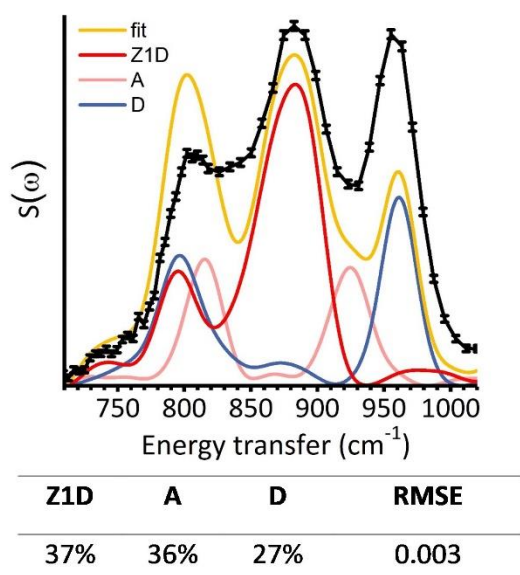


21

1 Figure 6. Representative contributions of different types of C-H corners, belonging to different models: *duo* (part a), *trio*  
2 (part b) and *quatro* (part c).

### 3 4.3. Linear combination fit with regular C-H components

4 To quantify, at least in relative terms, the abundance of the different C-H terminal geometries in a  
5 certain sample, we fitted the experimental INS spectra shown in Figure 1 with a linear combination  
6 of the simulated spectra discussed in section 4.2. Due to the limited number of experimental points  
7 compared to the number of possible C-H contributions from models, we had to limit the number of  
8 included functions. Consequently: 1) all the simulated spectra belonging to the same C-H termination  
9 category were averaged, reducing the number of possible contributions to eight cases; 2) T and Q  
10 corner sites were excluded from the fit analysis because they display too strong contributions in the  
11 730-800  $\text{cm}^{-1}$  region, where the experimental spectra are very weak; 3) the contributions of extended  
12 zigzag borders (Z1T, Z2 and Z3-4) always resulted in negligible values (much lower than 1%) when  
13 performing preliminary linear combination fit tests, and were thus excluded. Therefore, the  
14 experimental spectra were fitted with a linear combination of the simulated functions for Z1D, A and  
15 D terminations. The intensities of the spectra introduced in the linear combination were then  
16 normalised to account for a single C-H group.



17  
18 Figure 7. Result of the linear combination fit for the experimental spectrum of CwA (black) obtained by including the  
19 simulated functions of Z1D, A and D terminations. The best fit solution is reported in yellow, and the percentages of each  
20 component of the fit in the final result are reported in table form. The goodness of fit is evaluated by the RMSE.

21 Figure 7 shows the best fit (yellow) for the experimental spectrum of CwA (black) and the  
22 three different C-H contributions, complemented by a table summarising the resulting relative  
23 abundance of the C-H sites. Its Root Mean Square Error (RMSE) expresses the goodness of the fit.  
24 Although the three main bands characterizing the experimental spectrum are well reproduced in terms

1 of position, they are not reproduced in terms of relative intensities. In particular, if we renormalize  
2 the fitted and experimental spectra to the intensity of the band at  $800\text{ cm}^{-1}$ , the bands at  $850$  and  $955$   
3  $\text{cm}^{-1}$  are missing some intensity as well as additional contributions around  $830$  and  $930\text{ cm}^{-1}$  (i.e.  
4 where the experimental spectrum shows two minima) are not accounted for. Analogous results were  
5 obtained for all the other samples. Hence, it becomes clear that the fingerprint region of the INS  
6 experimental spectrum of a physically activated carbon cannot be fully reproduced by considering  
7 only regular C-H terminations.

#### 8 **4.4. DFT simulations of the INS spectra for physical defects**

9 Since activated carbons are by definition disordered and defective materials, the missing components  
10 in the fit reported in Figure 7 might be associated with defects. Defects may arise either because of  
11 the presence of heteroatoms (i.e. functional groups), or because of ruptures of the regularity in the  
12 aromatic domains (physical defects). Since physically activated carbons display a very low  
13 concentration of functional groups [17, 42], we focused on the latter class of defects. Although the  
14 number of possible physical defects is extremely high, we decided to focus on those containing C-H  
15 groups and hence detectable by INS.

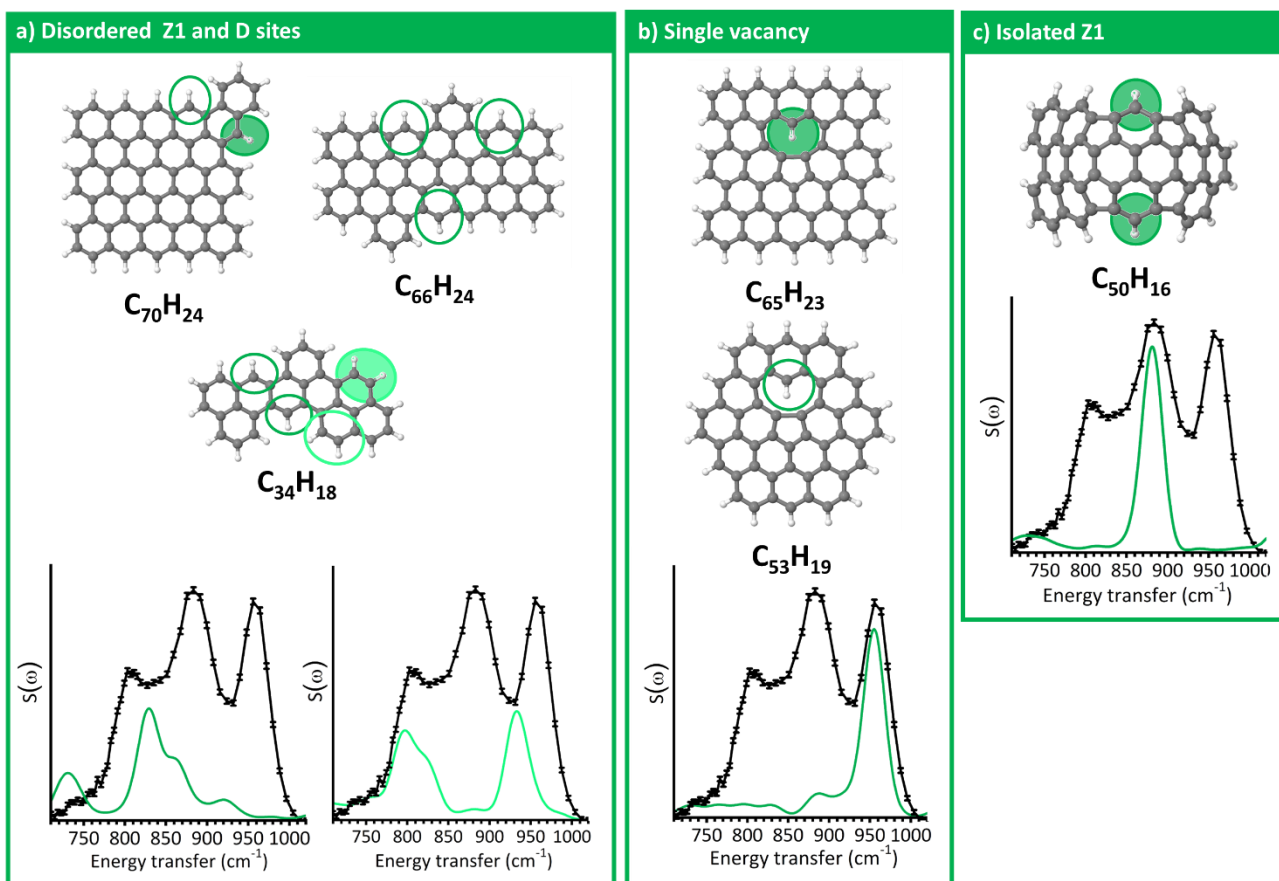
16 First, the aromatic models can simply include some disordered C-H terminations, hardly  
17 classifiable as any of the regular borders and corners classes described in section 4.2. For these  
18 disordered C-H terminations, the greatest variations in the INS spectra are observed for single zigzag  
19 sites, for which some examples are reported in Figure 8a, first plot. These terminations give a quite  
20 broad band centred at ca  $830\text{ cm}^{-1}$ , in correspondence with one of the minima of the experimental  
21 spectra. Disordered *duo* terminations instead (second plot in Figure 8a) give two main bands,  
22 similarly to the spectra of D and A terminations (Figure 5c and Figure 6a), but in this case the two  
23 bands fall at ca.  $800$  and  $935\text{ cm}^{-1}$ , about midway between the A and D regular cases. Generalizing,  
24 we can conclude that the INS fingerprint of terminations consisting in two C-H exposed at the same  
25 benzene ring fall within a continuum of cases, of which D and A sites correspond to the two extremes.  
26 Finally, T and Q corners are always inserted in peripheral positions in these models and hence they  
27 are not affected by disorder and/or defectivity of the model.

28 We also considered holes within the aromatic platelets and saturated by H atoms, since they  
29 have been recently demonstrated to occur in defective graphene [23]. Due to the limited size of the  
30 platelets in the activated carbons under investigation [17], only small holes can be imagined. Thus,  
31 we have focused on holes created by removing a single C atom from the model forming a five member  
32 ring and a C-H group (Figure 8b), which we labelled as a single vacancy. A distinct band in the  
33 fingerprint region at  $950\text{ cm}^{-1}$ , characterizes the simulated INS spectrum of this termination inside  
34 the hole.

1           A third kind of possible irregular termination consists in a single C-H site completely isolated  
2 from other C-H groups on adjacent benzene rings (Figure 8c). In this case, the considered C-H groups  
3 are isolated from their neighbours by the presence of four pentagonal rings. In this case, the out-of-  
4 plane bending mode of the C-H group has a very little tendency to combine with the vibrations of  
5 other C-H groups, resulting in a single and sharp band centred at ca 880 cm<sup>-1</sup>.

6           Activated carbons were also proposed to feature topological defects that introduce local  
7 curvature and sphericity within the graphenic planes [43]. We thus decided to simulate two additional  
8 models featuring the same kind of C-H terminations as model C<sub>54</sub>H<sub>18</sub> but with different curvatures,  
9 designed by introducing either a five or a seven-membered ring at the centre of the model. The  
10 analysis of their simulated spectra, shown in Figure S8 in the supporting information, immediately  
11 shows that the spectral features are almost undistinguishable from the corresponding flat model. This  
12 indicates that this region of the INS spectra is mostly sensible to the local geometry of the C-H  
13 terminations, and much less on defects not directly involving H atoms.

14           Three further simulations were run on models in which the source of the curvature (i.e. introduction  
15 of a 5-member ring) is located closer to the borders of the model, and so where it can directly affect  
16 the nearby C-H terminations. The characteristic INS spectral features of the three models are reported  
17 in Figure S9 in supporting information. The first two models were built starting from the hexagonal  
18 C<sub>54</sub>H<sub>18</sub> model, by adding five member rings at two distinct positions close to the border. For these  
19 models (Figure S9A and B), the Z1 and D terminations in close proximity with the five member rings  
20 show bands in the same frequency ranges and with similar intensities as the previously introduced  
21 disordered Z1 and D terminations on flat models of Figure 8a. Consequently, these curved models  
22 contribute to the disordered terminations similarly to the flat ones and we cannot distinguish in  
23 between them. The third model contains a five membered ring exposing one C-H termination. Its  
24 characteristic INS spectrum (Figure S9C) shows the most intense features in the 600-750 cm<sup>-1</sup> range,  
25 in correspondence with one of the minima of the experimental spectra. This observation makes us  
26 conclude that this specific termination is not expected to be significantly present in our samples.



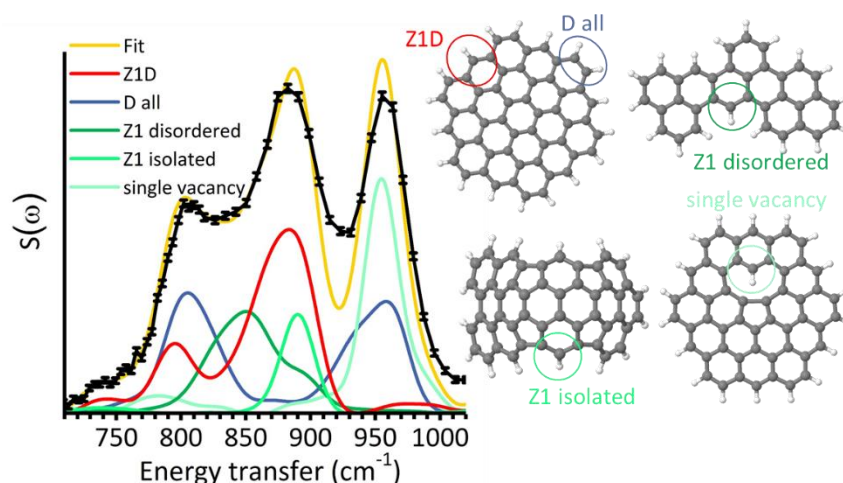
1  
 2 Figure 8. Disordered and defective models considered in this work and the characteristic contributions to the INS spectra  
 3 of their defective C-H terminations. The sites that behave differently than the regular ones are indicated by a circle. The  
 4 reported simulated INS spectra refer to the species highlighted with a full green circle. Part a): Models containing  
 5 disordered terminations, where disordered Z1 sites are circled in dark green and disordered D sites in light green. A  
 6 representative spectrum for both disordered Z1 and D sites is reported. Part b): Models containing a Single Vacancy  
 7 defect saturated by one H atom, and a representative spectrum of their INS contribution. Part c): Model containing an  
 8 isolated Z1 site, obtained by introducing four five membered rings and curvature in the model, and characteristic INS  
 9 spectrum of this site.

#### 10 4.5. Introduction of physical defects in the fit

11 With the simulations of the physical defects in the hands, we came back to the linear combination  
 12 analysis and added these new contributions to improve the fit result. To ensure the reliability of the  
 13 result we limited again as much as possible the number of functions included in the fit, and thus the  
 14 number of parameters to be optimised. At first, we decided to describe the D, A and disordered D  
 15 terminations with a single function (D-all), obtained by averaging their characteristic spectra. Then,  
 16 three new functions were added to the fit, accounting for disordered Z1, isolated Z1 and single  
 17 vacancy defects, obtained by averaging all the spectra belonging to the same category of C-H  
 18 terminations.

19 The new linear combination fit was therefore performed by including five functions Z1D, D-  
 20 all, disordered Z1, isolated Z1 and single vacancy, and imposing the following constrains: 1) the  
 21 concentration of regular terminations should be higher than that of irregular and defective sites; 2)  
 22 for the catalysts, the values of the coefficients in the fit should be equal or lower than those obtained

1 in the fit of the parent carbon. These choices were justified by the observation that the three main  
 2 peaks in the experimental spectra show a better matching with the spectra of regular terminations,  
 3 and that the intensity of the INS spectra for the catalysts is always less intense than for the parent  
 4 carbons. The result of this fit for CwA is shown in Figure 9. The same procedure was followed for  
 5 all the other activated carbons and catalysts, resulting in the final values reported in Table 3. For the  
 6 four activated carbons, all the coefficients obtained from the fit were normalised so that their sum  
 7 gives 100%, while all the results of the catalysts were normalised with respect to the parent support,  
 8 in order to allow a direct evaluation of the loss of hydrogen at the graphenic terminations as a  
 9 consequence of the metal deposition. The plots showing the results of the linear combination fit  
 10 analysis for the other samples are reported in Figure S10, S11, S12 and S13 in the supporting  
 11 information.



12

13 Figure 9: Result of the linear combination fit for the sample CwA. The best result was obtained by introducing in the  
 14 linear combination the functions for Z1D, D-all, disordered Z1, isolated Z1 and single vacancy sites. An example of a C-  
 15 H termination for each function in the fit is reported for clarity.

16 Table 3: Summary of the results of the linear combination fit on the experimental INS spectra of all the activated carbons  
 17 and catalysts. The values for the activated carbon supports are normalised so that their sum gives 100%, while those of  
 18 the catalysts were normalised with respect to the parent support. The goodness of the fit is evaluate by the RMSE.

	Z1D	D-all	Disordered Z1	Single vacancy	Isolated Z1	TOT	RMSE
	%	%	%	%	%		
<b>CwA</b>	25	38	19	12	5	100	0.001
<b>Pt(R)/CwA</b>	20	36	19	12	5	92	0.001
<b>Pd(NR)/CwA</b>	15	32	17	11	4	78	0.001
<b>Pd(R)/CwA</b>	13	32	19	11	4	79	0.002
<b>CwB</b>	28	33	23	11	5	100	0.001
<b>Pt(R)/CwB</b>	15	29	11	9	4	67	0.001
<b>CpA</b>	24	42	22	10	2	100	0.001
<b>Pt(R)/CpA</b>	16	35	18	9	2	78	0.001
<b>CpB</b>	27	41	20	11	2	100	0.001

Pt(R)/CpB | 18 36 19 11 2 86 0.001

As far as the bare carbons are concerned, the main C-H contributions are relatively similar for all the considered samples. In all the cases the experimental spectra are well reproduced by using mostly Z1D, D-all and disordered Z1 sites, followed by lower amounts of single vacancies, while the contribution of isolated Z1 sites is almost negligible. For all the four carbons, the main contribution is given by D-all sites, followed by Z1D and disordered Z1. The D-all sites are much more frequent in the activated carbons of peat origin than in those of wood origin. Among carbons with the same origin, the greatest difference is observed between CwA and CwB, and it is mostly reflected by the different D-all/Z1D ratio (1.5 and 1.2, respectively).

The deposition of Pd or Pt nanoparticles causes a small decrease in the total intensity of the spectra, as already observed in our previous experiment [5]. The result of the linear combination fit analysis allows us to evaluate which are the most affected C-H species: in fact, albeit the amount of all C-H sites decreases with respect to the parent carbon, the greatest variation is always observed for Z1D sites. For CwA, the perturbation caused by the deposition of Pt nanoparticles (sample Pt(R)/CwA) is relatively modest, with the greatest change observed for Z1D sites which decreased by about 5%. The deposition of Pd nanoparticles, instead, causes a much larger reduction of the regular C-H terminations, mostly evident for Z1D sites which decrease by about 10% in Pd(NR)/CwA, and by 12% for Pd(R)/CwA. These data also clearly indicate that the cause of the observed H loss in the catalysts is the deposition of the metal, and not the successive pre-reduction step. The most significant change was observed when depositing Pt nanoparticles on the CwB support, which resulted in a decrease of about 13% for Z1D sites and of about 12% for disordered Z1 sites. The effect of the Pt deposition is instead quite similar for the two carbons of peat origin, where the Z1D sites decreased of ca. 8-9% and the D-all decrease by about 5-7 %.

Even if the matching between the fitted solution and the experimental spectra increased significantly with the introduction of physical defects, it is evident for all the samples that the fits are still missing some contribution at about  $920\text{ cm}^{-1}$ , in correspondence with one of the minima of the experimental spectra. None of the defective models that we have simulated so far seems able to cover that region. Further simulations and experiments in this direction are planned.

## 5. Conclusions

In this work, we present the high-resolution INS spectra of four different activated carbons and of six industrial catalysts obtained by depositing Pd or Pt nanoparticles on the same carbons. The INS spectra contain information on the type and amount of the C-H terminations at the graphenic domains constituting the carbon. Albeit the investigated carbon supports show a certain degree of structural,

1 porous and morphological heterogeneity, the unprecedented high signal-to-noise ratio of our spectra in  
2 comparison with past measurements [17], allowed us to highlight tiny differences among carbons  
3 having different origins, and between the catalysts and the corresponding carbon supports. In  
4 particular, we observed that the deposition of the metal nanoparticles causes a general decrease of the  
5 C-H signals, which for Pt scales linearly with the metal dispersion: smaller the metal nanoparticles,  
6 larger is the amount of C-H affected by the metal deposition.

7 In order to interpret the differences observed in the experimental spectra, an extensive DFT  
8 study was performed. At first, we simulated the INS spectra of several aromatic models characterized  
9 by regular C-H terminations and/or by the presence of some physical defects. Successively, we  
10 determined the characteristic INS fingerprint of different C-H terminations. The experimental INS  
11 spectra were systematically fitted with a linear combination of five functions corresponding to: 1) C-  
12 H at regular zigzag borders and vicinal to a *duo* corner (Z1D); 2) C-H at regular armchair borders, at  
13 *duo* corners or at disordered *duo* terminations (D-all); 3) C-H at disordered zigzag borders (disordered  
14 Z1); 4) isolated C-H (isolated Z1); and 5) C-H in single vacancies inside the graphenic platelets. We  
15 found out that, although regular aromatic models are already able to reproduce the position of the  
16 experimental features, physical defects and disordered C-H species are necessary to obtain a good  
17 match between experimental and fitted spectra. We were not able to identify a general spectral  
18 fingerprint for the curvature and not planarity of the graphenic domains, but two of the defective  
19 contributions identified by linear combination analysis (Isolated Z1 and Single Vacancy) were indeed  
20 given by not planar models. Thus, it does not appear possible to describe in full the platelets structure  
21 within activated carbons considering flat geometries only.

22 The results of the fits indicate that the most frequent C-H terminations in all the activated  
23 carbons are D-all, followed by Z1D and disordered Z1, while the other two types of defects are much  
24 less frequent. The relative abundance of Z1D terminations is lower for carbons of peat origin (Cp)  
25 than for those of wood origin (Cw). Since the metal dispersion for catalysts prepared on Cp carbons  
26 is systematically lower than that on Cw carbons, these results suggest that the metal dispersion is  
27 improved on carbons having a large percentage of Z1D terminations. The decisive role of Z1D sites  
28 is confirmed by the observation that the metal nanoparticles deposition mainly affects this typology  
29 of C-H termination. These outcomes are particularly relevant for catalysis, since they offer for the  
30 first time an explanation of the relationship between the type of the carbon support and the metal  
31 dispersion. On a more general ground, this study demonstrates that high resolution INS spectra  
32 complemented by a systematic DFT study are invaluable tools for characterizing carbon-based  
33 materials.

34

## 1 Acknowledgments

2 This work was strongly encouraged from the beginning by our beloved Carlo Lamberti and Giuseppe  
3 Leofanti, to whom we will be infinitely grateful for having guided us with passion and enthusiasm.

4 We are also grateful to ILL for the time we have accounted on the computational cluster.

## 5 References

- 6 [1.] Rodríguez-Reinoso F., *Production and Applications of Activated Carbons*. Handbook of Porous Solids,  
7 2002: p. 1766-1827.
- 8 [2.] Fierro V., Torné-Fernández V., Montané D., and Celzard A., *Adsorption of phenol onto activated  
9 carbons having different textural and surface properties*. Microporous and Mesoporous Materials,  
10 2008. **111**(1): p. 276-284.
- 11 [3.] Sircar S., Golden T.C., and Rao M.B., *Activated carbon for gas separation and storage*. Carbon, 1996.  
12 **34**(1): p. 1-12.
- 13 [4.] Auer E., Freund A., Pietsch J., and Tacke T., *Carbons as supports for industrial precious metal catalysts*.  
14 Applied Catalysis A: General, 1998. **173**(2): p. 259-271.
- 15 [5.] Figueiredo J.L. and Pereira M.F.R., *The role of surface chemistry in catalysis with carbons*. Catalysis  
16 Today, 2010. **150**(1): p. 2-7.
- 17 [6.] Wang N., Li T., Song Y., Liu J., and Wang F., *Metal-free nitrogen-doped porous carbons derived from  
18 pomelo peel treated by hypersaline environments for oxygen reduction reaction*. Carbon, 2018. **130**:  
19 p. 692-700.
- 20 [7.] Qiu Y., Ali S., Lan G., Tong H., Fan J., Liu H., Li B., Han W., Tang H., Liu H., and Li Y., *Defect-rich activated  
21 carbons as active and stable metal-free catalyst for acetylene hydrochlorination*. Carbon, 2019. **146**:  
22 p. 406-412.
- 23 [8.] Li X., Duan X., Han C., Fan X., Li Y., Zhang F., Zhang G., Peng W., and Wang S., *Chemical activation of  
24 nitrogen and sulfur co-doped graphene as defect-rich carbocatalyst for electrochemical water  
25 splitting*. Carbon, 2019. **148**: p. 540-549.
- 26 [9.] Hao Y., Zhang X., Yang Q., Chen K., Guo J., Zhou D., Feng L., and Slanina Z., *Highly porous defective  
27 carbons derived from seaweed biomass as efficient electrocatalysts for oxygen reduction in both  
28 alkaline and acidic media*. Carbon, 2018. **137**: p. 93-103.
- 29 [10.] Qiu Z., Lin Y., Xin H., Han P., Li D., Yang B., Li P., Ullah S., Fan H., Zhu C., and Xu J., *Ultrahigh level  
30 nitrogen/sulfur co-doped carbon as high performance anode materials for lithium-ion batteries*.  
31 Carbon, 2018. **126**: p. 85-92.
- 32 [11.] Girgis B.S., Yunis S.S., and Soliman A.M., *Characteristics of activated carbon from peanut hulls in  
33 relation to conditions of preparation*. Materials Letters, 2002. **57**(1): p. 164-172.
- 34 [12.] de Lima L.S., Quináia S.P., Melquiades F.L., de Biasi G.E.V., and Garcia J.R., *Characterization of  
35 activated carbons from different sources and the simultaneous adsorption of Cu, Cr, and Zn from  
36 metallurgic effluent*. Separation and Purification Technology, 2014. **122**: p. 421-430.
- 37 [13.] Lazzarini A., Pellegrini R., Piovano A., Rudić S., Castan-Guerrero C., Torelli P., Chierotti M.R., Gobetto  
38 R., Lamberti C., and Groppo E., *The effect of surface chemistry on the performances of Pd-based  
39 catalysts supported on activated carbons*. Catalysis Science & Technology, 2017. **7**(18): p. 4162-4172.
- 40 [14.] Yan P., Zhang B., Wu K.-H., Su D., and Qi W., *Surface chemistry of nanocarbon: Characterization  
41 strategies from the viewpoint of catalysis and energy conversion*. Carbon, 2019. **143**: p. 915-936.
- 42 [15.] Albers P.W., Pietsch J., Krauter J., and Parker S.F., *Investigations of activated carbon catalyst supports  
43 from different natural sources*. Physical Chemistry Chemical Physics, 2003. **5**(9): p. 1941-1949.
- 44 [16.] Albers P.W., Weber W., Möbus K., Wieland S.D., and Parker S.F., *Neutron scattering study of the  
45 terminating protons in the basic structural units of non-graphitising and graphitising carbons*. Carbon,  
46 2016. **109**: p. 239-245.
- 47 [17.] Lazzarini A., Piovano A., Pellegrini R., Leofanti G., Agostini G., Rudić S., Chierotti M.R., Gobetto R.,  
48 Battiato A., Spoto G., Zecchina A., Lamberti C., and Groppo E., *A comprehensive approach to*

- 1 *investigate the structural and surface properties of activated carbons and related Pd-based catalysts.*  
2 Catalysis Science & Technology, 2016. **6**(13): p. 4910-4922.
- 3 [18.] Carosso M., Lazzarini A., Piovano A., Pellegrini R., Morandi S., Manzoli M., Vitillo J.G., Ruiz M.J.,  
4 Lamberti C., and Groppo E., *Looking for the active hydrogen species in a 5 wt% Pt/C catalyst: a*  
5 *challenge for inelastic neutron scattering.* Faraday Discussions, 2018. **208**(0): p. 227-242.
- 6 [19.] Albers P., Seibold K., Prescher G., Freund B., Parker S.F., Tomkinson J., Ross D.K., and Fillaux F.,  
7 *Neutron spectroscopic investigations on different grades of modified furnace blacks and gas blacks.*  
8 Carbon, 1999. **37**(3): p. 437-444.
- 9 [20.] Fillaux F., Papoular R., Lautié A., and Tomkinson J., *Inelastic neutron-scattering study of the proton*  
10 *dynamics in carbons and coals.* Carbon, 1994. **32**(7): p. 1325-1331.
- 11 [21.] Parker S.F., Imberti S., Callear S.K., and Albers P.W., *Structural and spectroscopic studies of a*  
12 *commercial glassy carbon.* Chemical Physics, 2013. **427**: p. 44-48.
- 13 [22.] Natkaniec I., Sheka E.F., Druzbicki K., Hołderna-Natkaniec K., Gubin S.P., Buslaeva E.Y., and Tkachev  
14 S.V., *Computationally Supported Neutron Scattering Study of Parent and Chemically Reduced*  
15 *Graphene Oxide.* The Journal of Physical Chemistry C, 2015. **119**(32): p. 18650-18662.
- 16 [23.] Cavallari C., Pontiroli D., Jiménez-Ruiz M., Johnson M., Aramini M., Gaboardi M., Parker S.F., Riccò  
17 M., and Rols S., *Hydrogen motions in defective graphene: the role of surface defects.* Physical  
18 Chemistry Chemical Physics, 2016. **18**(36): p. 24820-24824.
- 19 [24.] Piovano A., Lazzarini A., Pellegrini R., Leofanti G., Agostini G., Rudić S., Bugaev A.L., Lamberti C., and  
20 Groppo E., *Progress in the Characterization of the Surface Species in Activated Carbons by means of*  
21 *INS Spectroscopy Coupled with Detailed DFT Calculations.* Advances in Condensed Matter Physics,  
22 2015. **2015**.
- 23 [25.] Pellegrini R., Leofanti G., Agostini G., Groppo E., Rivallan M., and Lamberti C., *Pd-Supported Catalysts:*  
24 *Evolution of Support Porous Texture along Pd Deposition and Alkali-Metal Doping.* Langmuir, 2009.  
25 **25**(11): p. 6476-6485.
- 26 [26.] Agostini G., Groppo E., Piovano A., Pellegrini R., Leofanti G., and Lamberti C., *Preparation of*  
27 *Supported Pd Catalysts: From the Pd Precursor Solution to the Deposited Pd<sup>2+</sup> Phase.* Langmuir, 2010.  
28 **26**(13): p. 11204-11211.
- 29 [27.] Kaprielova K.M., Yakovina O.A., Ovchinnikov I.I., Koscheev S.V., and Lisitsyn A.S., *Preparation of*  
30 *platinum-on-carbon catalysts via hydrolytic deposition: Factors influencing the deposition and*  
31 *catalytic properties.* Applied Catalysis A: General, 2012. **449**: p. 203-214.
- 32 [28.] Anderson J.R. and Pratt K.C., *Introduction to Characterization and Testing of Catalysts.* 1986, Sydney,  
33 Australia: Academic Press.
- 34 [29.] Agostini G., Pellegrini R., Leofanti G., Bertinetti L., Bertarione S., Groppo E., Zecchina A., and Lamberti  
35 C., *Determination of the Particle Size, Available Surface Area, and Nature of Exposed Sites for*  
36 *Silica–Alumina-Supported Pd Nanoparticles: A Multitechnical Approach.* The Journal of Physical  
37 Chemistry C, 2009. **113**(24): p. 10485-10492.
- 38 [30.] Jiménez-Ruiz M., Ivanov A., and Fuard S., *LAGRANGE - the new neutron vibrational spectrometer at*  
39 *the ILL.* Journal of Physics: Conference Series, 2014. **549**: p. 012004.
- 40 [31.] [dataset] Piovano A., Agostini G., Carosso M., Groppo E., Jimenez Ruiz M., Lamberti C., Lazzarini A.,  
41 Manzoli M., Morandi S., Pellegrini R., and Vottero E., *Study of the Pt-hydride formation and spillover*  
42 *effect on Pt/Al<sub>2</sub>O<sub>3</sub> and Pt/C catalysts DOI:10.5291/ILL-DATA.7-05-466,* 2016.
- 43 [32.] [dataset] Vottero E., Carosso M., Groppo E., Jimenez Ruiz M., Lamberti C., Pellegrini R., and Piovano  
44 A., *Exploring the surface chemistry of activated carbons by INS and DFT calculations DOI:10.5291/ILL-*  
45 *DATA.7-04-162,* 2018.
- 46 [33.] Dovesi R., Erba A., Orlando R., Zicovich-Wilson C.M., Civalleri B., Maschio L., Rérat M., Casassa S.,  
47 Baima J., Salustro S., and Kirtman B., *Quantum-mechanical condensed matter simulations with*  
48 *CRYSTAL.* Wiley Interdisciplinary Reviews: Computational Molecular Science, 2018. **8**(4).
- 49 [34.] Ramirez-Cuesta A.J., *aCLIMAX 4.0.1, The new version of the software for analyzing and interpreting*  
50 *INS spectra.* Computer Physics Communications, 2004. **157**(3): p. 226-238.
- 51 [35.] Becke A.D., *Density-functional thermochemistry. III. The role of exact exchange.* The Journal of  
52 Chemical Physics, 1993. **98**(7): p. 5648-5652.

- 1 [36.] Lee C., Yang W., and Parr R.G., *Development of the Colle-Salvetti correlation-energy formula into a*  
2 *functional of the electron density*. Physical Review B, 1988. **37**(2): p. 785-789.
- 3 [37.] Maschio L., Lorenz M., Pullini D., Sgroi M., and Civalieri B., *The unique Raman fingerprint of boron*  
4 *nitride substitution patterns in graphene*. Physical Chemistry Chemical Physics, 2016. **18**(30): p.  
5 20270-20275.
- 6 [38.] Kar T., Scheiner S., Adhikari U., and Roy A.K., *Site Preferences of Carboxyl Groups on the Periphery of*  
7 *Graphene and Their Characteristic IR Spectra*. The Journal of Physical Chemistry C, 2013. **117**(35): p.  
8 18206-18215.
- 9 [39.] Alcolea Palafox M., *Scaling Factors for the Prediction of Vibrational Spectra. I. Benzene Molecule*.  
10 International Journal of Quantum Chemistry, 2000. **77**(3): p. 661-684.
- 11 [40.] Centrone A., Brambilla L., Renouard T., Gherghel L., Mathis C., Müllen K., and Zerbi G., *Structure of*  
12 *new carbonaceous materials: The role of vibrational spectroscopy*. Carbon, 2005. **43**(8): p. 1593-1609.
- 13 [41.] Zander M., *Die Herstellung von Polycyclischen Aromaten*, in *Polycyclische Aromaten:*  
14 *Kohlenwasserstoffe und Fullerene*, Zander M., Editor. 1995, Vieweg+Teubner Verlag: Wiesbaden. p.  
15 158-187.
- 16 [42.] Figueiredo J.L., Pereira M.F.R., Freitas M.M.A., and Órfão J.J.M., *Modification of the surface chemistry*  
17 *of activated carbons*. Carbon, 1999. **37**(9): p. 1379-1389.
- 18 [43.] Harris P.J.F., *Fullerene-like models for microporous carbon*. Journal of Materials Science, 2013. **48**(2):  
19 p. 565-577.

20

21